tail) and the N terminus of cortical cytoskeleton-associated protein of ~23 kD ($CAP23_{20}$). We also assayed the kinase-associated 1 (KA1) domain from microtubule-associated protein–microtubule affinity–regulating kinase 1 (MARK1), which interacts nonspecifically with acidic lipids (*23*). In all cases, combined removal of PI4P and $PI(4,5)P_2$ caused depletion of the proteins from the PM (Fig. 4A and fig. S7), with little effect when either lipid was depleted alone (*13*). Proteins that retained a secondary membrane targeting motif, such as prenylated K-Ras tail, were still found in the PM but were no longer enriched there compared with the amounts in other [presumably negatively charged (*22*)] membranes (Fig. 4A and fig. S8A). These effects were due to nonspecific electrostatic interactions, because no effect was seen on the PS-specific lactadherin C2 domain (*22*) or the C terminus of H-Ras, which interacts with the membrane solely through its hydrophobic lipid moieties (Fig. 4A and fig. S7). Measuring K-Ras tail's PM dissociation rate by fluorescence recovery after photobleaching (*24*) after PI4P and/or $PI(4,5)P_2$ depletion revealed that the two lipids made similar contributions to the protein's electrostatic interactions with the PM in vivo (fig. S8).

$PI(4,5)P_2$ has been proposed to be a molecular switch that restricts the activity of several ion channels to the PM (*25*), a phenomenon that can be highly specific for $PI(4,5)P_2$ (*1*, *26*–*28*). We wondered whether this is typical for all channels or whether some have a more general polyanionic lipid requirement, which can also be fulfilled by PI4P. For example, the heat and capsaicin-activated transient receptor potential vanilloid 1 (TRPV1) cation channel can be both inhibited and activated by $PI(4,5)P_2$ and possibly PI4P (*29*). Translocation of PJ-Sac or INPP5E had no effect on prolonged (Fig. 4, B to D) or repetitive (fig. S9) capsaicin activation of TRPV1, but it was inhibited when both PI4P and $PI(4,5)P_2$ were depleted by PJ (Fig. 4, B to D, and fig. S9). Therefore, it appears that either lipid is sufficient for TRPV1 channel activity. However, this does not apply to all lipid-activated cation channels. For example, the menthol-activated transient receptor potential melatastatin 8 (TRPM8) channel is specifically dependent on $PI(4,5)P_2$ (*12*) and was inhibited by $PI(4,5)P_2$ depletion, but not by removing PI4P with PJ-Sac (Fig. 4, E to G).

Our results reveal an unanticipated role for PI4P at the PM of cells: Most of it is not required to support synthesis of $PI(4,5)P_2$. Rather, PI4P makes an autonomous contribution to the polyanionic lipid pool that defines the inner leaflet of the PM, a function it shares with $PI(4,5)P_2$. We suggest that PI4P fulfills the need of any PM functions that simply require polyvalent anionic lipids. This leaves $PI(4,5)P_2$ free to undergo rapid turnover and regulate its large repertoire of specific effector proteins, which may decrease its effective free concentration, without deleteriously perturbing the unique and defining electrostatic properties of the PM.

References and Notes

1. B.-C. Suh, B. Hille, *Curr. Opin. Neurobiol.* **15**, 370 (2005).
2. G. Di Paolo, P. De Camilli, *Nature* **443**, 651 (2006).
3. S. McLaughlin, D. Murray, *Nature* **438**, 605 (2005).
4. T. R. Graham, C. G. Burd, *Trends Cell Biol.* **21**, 113 (2011).
5. G. R. V. Hammond, G. Schiavo, R. F. Irvine, *Biochem. J.* **422**, 23 (2009).
6. D. Sarkes, L. E. Rameh, *Biochem. J.* **428**, 375 (2010).
7. A. Balla *et al.*, *Mol. Biol. Cell* **19**, 711 (2008).
8. G. B. Willars, S. R. Nahorski, R. A. Challiss, *J. Biol. Chem.* **273**, 5037 (1998).
9. J. Clark *et al.*, *Nat. Methods* **8**, 267 (2011).
10. P. Várnai, T. Balla, *J. Cell Biol.* **143**, 501 (1998).
11. L. R. Stephens, T. R. Jackson, P. T. Hawkins, *Biochim. Biophys. Acta* **1179**, 27 (1993).
12. P. Várnai, B. Thyagarajan, T. Rohacs, T. Balla, *J. Cell Biol.* **175**, 377 (2006).
13. W. D. Heo *et al.*, *Science* **314**, 1458 (2006).
14. S. Guo, L. E. Stolz, S. M. Lemrow, J. D. York, *J. Biol. Chem.* **274**, 12990 (1999).
15. P. S. McPherson *et al.*, *Nature* **379**, 353 (1996).
16. A. Roy, T. P. Levine, *J. Biol. Chem.* **279**, 44683 (2004).
17. Z. Szentpetery, A. Balla, Y. J. Kim, M. A. Lemmon, T. Balla, *BMC Cell Biol.* **10**, 67 (2009).
18. C. N. Antonescu, F. Aguet, G. Danuser, S. L. Schmid, *Mol. Biol. Cell* **22**, 2588 (2011).
19. L. F. Horowitz *et al.*, *J. Gen. Physiol.* **126**, 243 (2005).
20. Z. Szentpetery, P. Várnai, T. Balla, *Proc. Natl. Acad. Sci. U.S.A.* **107**, 8225 (2010).
21. T. Yeung *et al.*, *Science* **313**, 347 (2006).
22. T. Yeung *et al.*, *Science* **319**, 210 (2008).
23. K. Moravcevic *et al.*, *Cell* **143**, 966 (2010).
24. G. R. V. Hammond, Y. Sim, L. Lagnado, R. F. Irvine, *J. Cell Biol.* **184**, 297 (2009).
25. D. W. Hilgemann, S. Feng, C. Nasuhoglu, *Sci. STKE* **2001**, re19 (2001).
26. N. D'Avanzo, W. W. L. Cheng, D. A. Doyle, C. G. Nichols, *J. Biol. Chem.* **285**, 37129 (2010).
27. M. R. Whorton, R. MacKinnon, *Cell* **147**, 199 (2011).
28. S. B. Hansen, X. Tao, R. MacKinnon, *Nature* **477**, 495 (2011).
29. V. Lukacs *et al.*, *J. Neurosci.* **27**, 7070 (2007).

Acknowledgments: We thank M. Lemmon, K. Moravcevic, D. Oliver, D. D. Saur, and L. Stephens for helpful discussions and constructs. G.R.V.H. and R.F.I. were supported by the Wellcome Trust and the Isaac Newton Trust, M.J.F. by the Alexander von Humboldt Foundation and the Isaac Newton Trust, K.E.A. by the UK Biotechnology and Biological Sciences Research Council, A.K. by a Dame Rosemary Murray Scholarship, and T.B. by the Intramural Research Program of the Eunice Kennedy Shriver National Institute of Child Health and Human Development (NICHD), NIH. We thank V. Schram of the NICHD Microscopy and Imaging Core for technical assistance with fluorescence recovery after photobleaching experiments. Constructs used in this work are available from www.addgene.com.

Supplementary Materials

www.sciencemag.org/cgi/content/full/science.1222483/DC1
Materials and Methods
Figs. S1 to S9
References (*30*–*37*)

27 March 2012; accepted 12 June 2012
Published online 21 June 2012;
10.1126/science.1222483

Lineage Tracing Reveals $Lgr5^+$ Stem Cell Activity in Mouse Intestinal Adenomas

Arnout G. Schepers,* Hugo J. Snippert,*† Daniel E. Stange, Maaike van den Born, Johan H. van Es, Marc van de Wetering, Hans Clevers‡

The concept that tumors are maintained by dedicated stem cells, the so-called cancer stem cell hypothesis, has attracted great interest but remains controversial. Studying mouse models, we provide direct, functional evidence for the presence of stem cell activity within primary intestinal adenomas, a precursor to intestinal cancer. By "lineage retracing" using the multicolor Cre-reporter *R26R-Confetti*, we demonstrate that the crypt stem cell marker Lgr5 (leucine-rich repeat–containing heterotrimeric guanine nucleotide–binding protein–coupled receptor 5) also marks a subpopulation of adenoma cells that fuel the growth of established intestinal adenomas. These $Lgr5^+$ cells, which represent about 5 to 10% of the cells in the adenomas, generate additional $Lgr5^+$ cells as well as all other adenoma cell types. The $Lgr5^+$ cells are intermingled with Paneth cells near the adenoma base, a pattern reminiscent of the architecture of the normal crypt niche.

Intestinal tumorigenesis is thought to result from sequentially acquired mutations in specific genes, driving progression from premalignant precursor lesions called adenomas to invasive malignancies (*1*). Adenomas are formed by mutational activation of the Wnt signaling pathway, most notably by loss of the *APC* (*adenomatous polyposis coli*) tumor suppressor gene (*2*). By using the knock-in allele $Lgr5^{EGFP\text{-}Ires\text{-}CreERT2}$, we have shown that the cell surface receptor Lgr5 (leucine-rich repeat–containing heterotrimeric guanine nucleotide–binding protein–coupled receptor 5) marks normal tissue stem cells in stomach, small intestine, colon, and hair follicles (*3*). This allele allows visualization of $Lgr5^+$ stem cells by GFP (green fluorescent protein). Moreover,

Hubrecht Institute, Koninklijke Nederlandse Akademie van Wetenschappen, and University Medical Center Utrecht, Uppsalalaan 8, 3584 CT Utrecht, Netherlands.

*These authors contributed equally to this work.
†Present address: Molecular Cancer Research, Centre of Biomedical Genetics and Cancer Genomics Centre, University Medical Center Utrecht, Universiteitsweg 100, 3584 CG Utrecht, Netherlands.
‡To whom correspondence should be addressed. E-mail: h.clevers@hubrecht.eu

Downloaded from www.sciencemag.org on August 12, 2012

the coexpressed Cre fusion protein can be activated at will in these stem cells by tamoxifen injection and will then recombine two adjacent LoxP sites When a so-called Cre reporter allele is crossed into the *Lgr5* knock-in mouse strain, tamoxifen injection can result in a visible change (e.g., a color) in an individual Lgr5$^+$ cell that is inherited by all of its daughter cells. This strategy to document the behavior of stem cells is called lineage tracing. Although deletion of *Apc* in other cells of the intestinal epithelium does not lead to adenoma formation, we have shown that Apc-mutant Lgr5$^+$ stem cells form progressively growing adenomas (*4*). Comparable adenomas were obtained by using another Cre driver (i.e., *CD133*^{CreERT2}) to induce *Apc* gene deletion in these same stem cells (*5*). We noted that macroscopic adenomas in these mice contained low numbers of Lgr5$^+$ cells, suggesting the preservation of a stem cell hierarchy within the tumors (*4*).

To investigate the existence of such a cellular hierarchy in adenomas, we exploited the multicolor Cre reporter termed *R26R-Confetti* (*6*). When *R26R-Confetti* is crossed into the *Lgr5* knock-in mouse strain, tamoxifen injection will allow single Lgr5$^+$ stem cells to randomly adopt one of the four fluorescent colors encoded in the *R26R-Confetti* allele. Of importance for the current study, two of the four colors remain in the *R26R-Confetti* allele after tamoxifen injection (blue with red or green with yellow). One of these is active, the other silent (Fig. 1A). In theory, a second tamoxifen injection can induce "flipping" from the active color to the silent color (here termed retracing). To test this, we globally activated *R26R-Confetti* in the intestinal epithelium by using the β-naphtoflavone–inducible *Ah-Cre* mouse strain (*7*). As hypothesized, the already rearranged *R26R-Confetti* reporter could be flipped to the remaining color by a second tamoxifen injection (fig. S1). Spontaneous color conversions were never observed.

To study the behavior of Lgr5$^+$ cells within *Apc*-mutant adenomas, we then crossed *Lgr5*$^{EGFP\text{-}Ires\text{-}CreERT2}$/*Apc*$^{fl/fl}$ mice with the *R26R-Confetti* strain. Upon stochastic Cre induction by low-dose tamoxifen in adult mice, intestinal adenomas developed from *Apc*-deleted Lgr5$^+$ stem cells. After 4 weeks, we observed large adenomas (fig. S2, A to C) that either uniformly expressed a single *Confetti* color or consisted of anatomically separate segments that were each marked uniformly in a single *Confetti* color (Fig. 1B). The latter result indicates that such large adenomas were derived from several independent *Apc*-mutant stem cells, most likely located in adjacent crypts. Indeed, such segmental oligo-clonality of adenomas has been described (*8*, *9*). Of note, recombination of the floxed *Apc* allele was more efficient than the activation of *R26R-Confetti* in

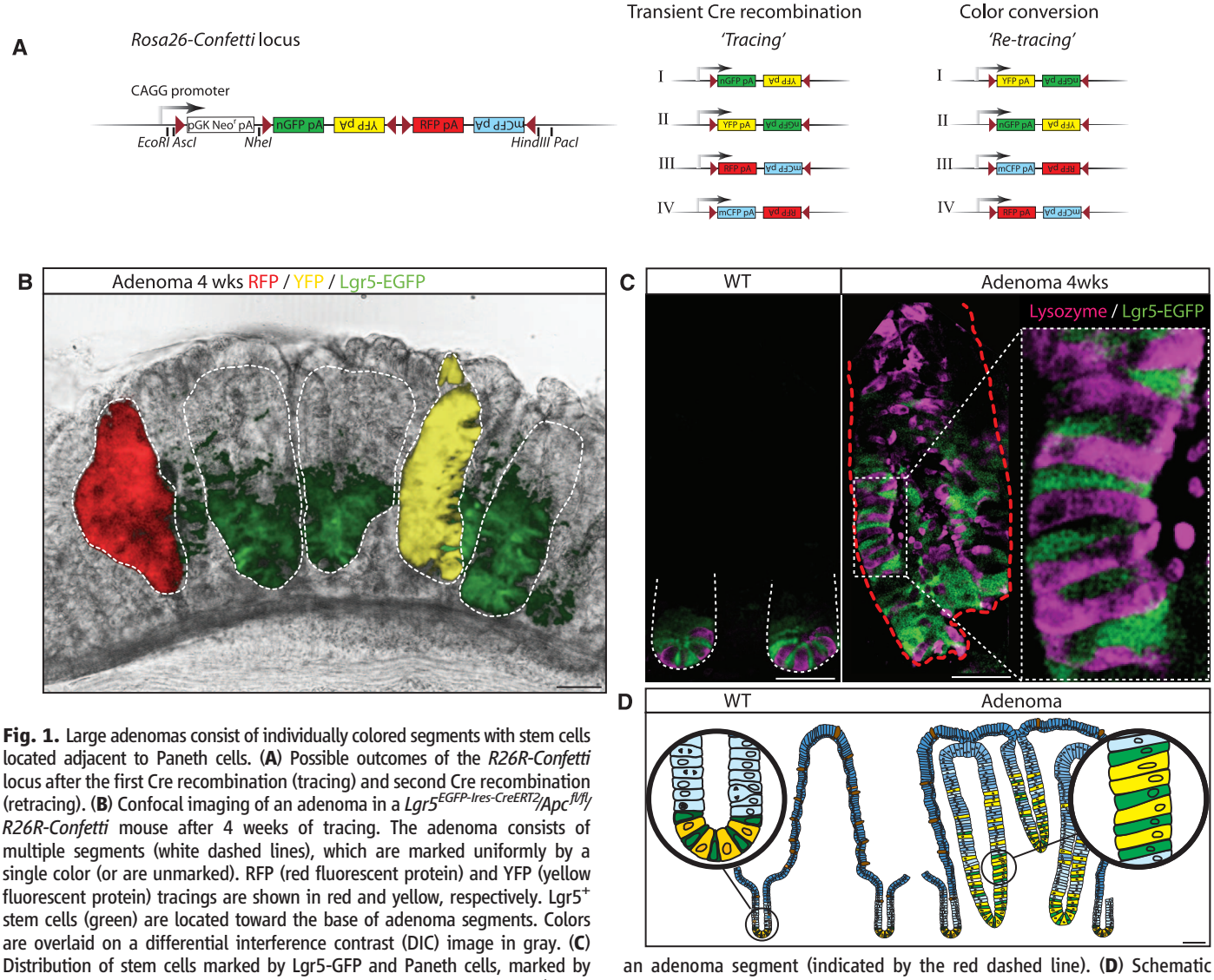

Fig. 1. Large adenomas consist of individually colored segments with stem cells located adjacent to Paneth cells. (**A**) Possible outcomes of the *R26R-Confetti* locus after the first Cre recombination (tracing) and second Cre recombination (retracing). (**B**) Confocal imaging of an adenoma in a *Lgr5*$^{EGFP\text{-}Ires\text{-}CreERT2}$/*Apc*$^{fl/fl}$/*R26R-Confetti* mouse after 4 weeks of tracing. The adenoma consists of multiple segments (white dashed lines), which are marked uniformly by a single color (or are unmarked). RFP (red fluorescent protein) and YFP (yellow fluorescent protein) tracings are shown in red and yellow, respectively. Lgr5$^+$ stem cells (green) are located toward the base of adenoma segments. Colors are overlaid on a differential interference contrast (DIC) image in gray. (**C**) Distribution of stem cells marked by Lgr5-GFP and Paneth cells, marked by lysozyme (purple) at the base of wild-type (WT) crypts (left). (Right) Lgr5$^+$ stem cells (green) are located adjacent to Paneth cells (purple) toward the base of an adenoma segment (indicated by the red dashed line). (**D**) Schematic representation of the intermingled stem cells and Paneth cells in wild-type crypts (left) and adenomas (right). Scale bars indicate 50 μm.

Downloaded from www.sciencemag.org on August 12, 2012

the same stem cell, because not all adenomas or adenoma segments expressed a *Confetti* color.

In normal small intestinal crypts, stem cells are always adjacent to Paneth cells. These Paneth cells serve as niche cells to the stem cells by producing signaling molecules such as Wnt, epidermal growth factor (EGF), and Notch ligands (*10*). The *Apc*-mutant adenomas contained Paneth cells (Fig. 1C) but typically lacked mature goblet cells and enterocytes (fig. S2, D and E). Lgr5^{+} adenoma cells were often located adjacent to adenoma Paneth cells, suggesting the existence of an adenoma stem cell niche (Fig. 1C). Indeed, these clusters of Lgr5^{+} cells and Paneth cells tended to be located toward the base of the wedge-shaped adenoma segments, a situation reminiscent of normal crypt architecture (Fig. 1D). We noted a similar arrangement in colon adenomas, in which areas of Lgr5^{+} cells coincided with the location of the colon-counterpart of the Paneth cell, the deep crypt secretory cell, marked by Reg4 (*10*, *11*) (fig. S3). To mimic the next step in the tumorigenic process, we additionally crossed in an allele of K-ras that can be oncogenically activated by Cre (*K-ras*$^{LSL-G12D}$) (*12*). We observed a dramatic acceleration of the growth of these *Apc/Kras* mutant tumors compared with *Apc*-mutant adenomas. The mice became moribund within 7 to 10 days, yet the cryptlike architecture was preserved in the *Apc/Kras* double-mutant tumors (fig. S4).

Next, we set out to determine the transcriptional profile of Lgr5-GFP^{hi} cells in adenomas to allow comparison to normal crypt Lgr5-GFP^{hi} stem cells. We sorted Lgr5-GFP^{hi} and Lgr5-GFP^{lo} cells from 30-day-old adenomas and performed comparative gene expression analyses of the two populations. Gene set enrichment analyses demonstrated that the Lgr5-GFP^{hi} stem cell signature determined for normal crypts (*13*) was strongly enriched in the Lgr5-GFP^{hi} adenoma cells (Fig. 2). This observation suggested that the Lgr5-GFP^{hi} adenoma cells retain stem cell properties. To substantiate this notion, we compared the clonogenic potential of Lgr5-GFP^{hi} and Lgr5-GFP^{lo} adenoma cells in a defined culture system developed for normal tissue Lgr5-GFP^{hi} stem cells (*14*, *15*). In this assay, normal Lgr5-GFP^{hi} cells grow out into crypt-villus organoids, whereas Lgr5-GFP^{lo} rarely grow out, consistent with the idea that Lgr5-GFP^{hi} cells constitute multipotent stem cells. Analysis of the clonogenic potential of Lgr5-GFP^{hi} and Lgr5-GFP^{lo} adenoma cells in this culture system recapitulated the observations made in normal tissue: The colony-forming efficiency of Lgr5-GFP^{hi} adenoma cells was about 20 times greater than that of Lgr5-GFP^{lo} adenoma cells (Fig. 2, D and E).

To trace the fate of Lgr5^{+} adenoma cells in vivo, we injected 10-week-old *Lgr5*$^{EGFP\text{-}Ires\text{-}CreERT2}$/*Apc*$^{fl/fl}$/*R26R-Confetti* mice with tamoxifen. After allowing *Confetti*-marked adenomas to develop for 24 days, we induced lineage retracing by a second tamoxifen injection. Adenomas were analyzed by confocal microscopy at different time points after the second Cre pulse. We observed rare retracings within large adenomas (~six color retracings per 100 adenoma segments), which invariably involved switching to the silent color in that particular adenoma. As an example, rare blue cells were observed within red adenomas early after lineage tracing (Fig. 3). Because we observed retracing events in only ~6% of *Confetti*-marked adenomas and these presented typically as a single cell at one day after the second tamoxifen

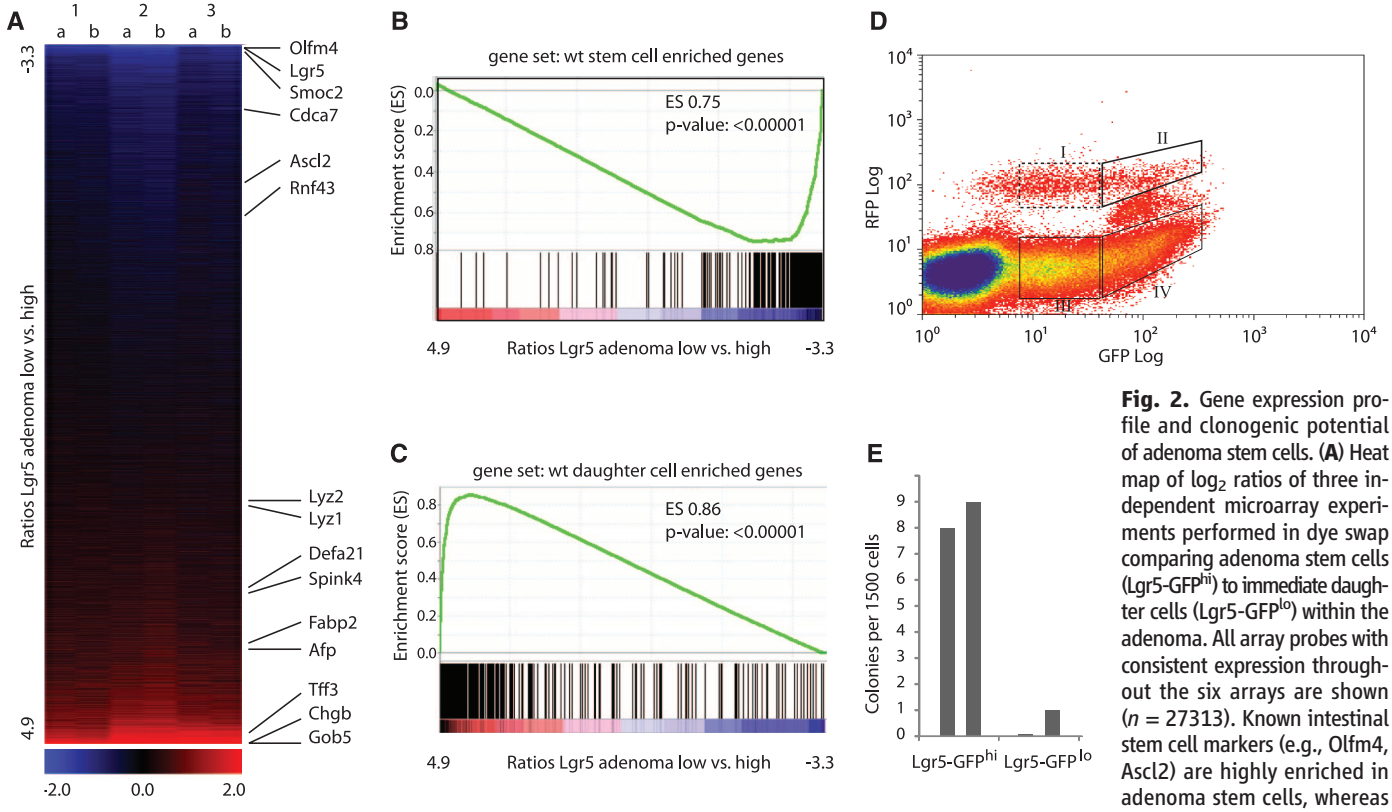

Fig. 2. Gene expression profile and clonogenic potential of adenoma stem cells. (**A**) Heat map of $\log_2$ ratios of three independent microarray experiments performed in dye swap comparing adenoma stem cells (Lgr5-GFP^{hi}) to immediate daughter cells (Lgr5-GFP^{lo}) within the adenoma. All array probes with consistent expression throughout the six arrays are shown (n = 27313). Known intestinal stem cell markers (e.g., Olfm4, Ascl2) are highly enriched in adenoma stem cells, whereas their daughter cells express markers for the four cell lineages in the gut: goblet cells (Gob5, Tff3), enteroendocrine cells (Chgb), enterocytes (Fabp2, Afp), and Paneth cells (Lyz1/2, Dfa21). (**B**) Gene set enrichment analysis (GSEA). Genes are ranked according to their differential expression between Lgr5-GFP^{lo} cells and Lgr5-GFP^{hi} cells. Black bars below the graph depict the position of 291 genes significantly enriched in normal Lgr5^{+} intestinal stem cells [GEO data set GSE23672 (*13*)]. A highly significant enrichment of this gene set was detected toward the genes highly expressed in Lgr5-GFP^{hi} adenoma cells. (**C**) GSEA analysis on the same data set as in (B), now analyzed for the top 500 genes significantly enriched in daughter cells of normal Lgr5^{+} stem cells. A highly significant enrichment of this gene set was detected toward the genes with higher expression in Lgr5-GFP^{lo} adenoma cells. ES, enrichment score. (**D**) Fluorescence-activated cell sorting profile of *Lgr5-EGFP-Ires-CreERT2/Apc*$^{fl/fl}$*/R26R-Confetti* mice 7 days after induction. Cells positive for RFP are adenoma cells. Gates I and II represent the Lgr5-GFP^{lo} and Lgr5-GFP^{hi} adenoma cells, respectively. Gates III and IV represent WT Lgr5-GFP^{lo} and Lgr5-GFP^{hi} cells. (**E**) Colony-forming efficiency of sorted adenoma cells. The outgrowth efficiency of Lgr5-GFP^{hi} adenoma cells is about 20 times higher than that of Lgr5-GFP^{lo} adenoma cells.

Downloaded from www.sciencemag.org on August 12, 2012

injection (Fig. 3, D and E), we considered these to represent clonal retracing events. In other words, these cells were derived from a single adenoma stem cell. As expected, the blue cells were mostly located near the base of the wedge-shaped adenoma segments, the location of the Lgr5^{+} cells. No spontaneous color conversion was observed in control mice that were not given a second Cre pulse, in a total of 107 adenomas analyzed 27 days after one pulse of tamoxifen.

Six days after retracing, the number of blue cells within red adenomas had increased. Moreover, the growing blue clones presented as ribbonlike structures emanating from the base of the segments and projecting toward to the intestinal lumen (Fig. 3B), thus resembling, in a crude and somewhat chaotic way, the more-organized tracing patterns observed in healthy intestinal tissue

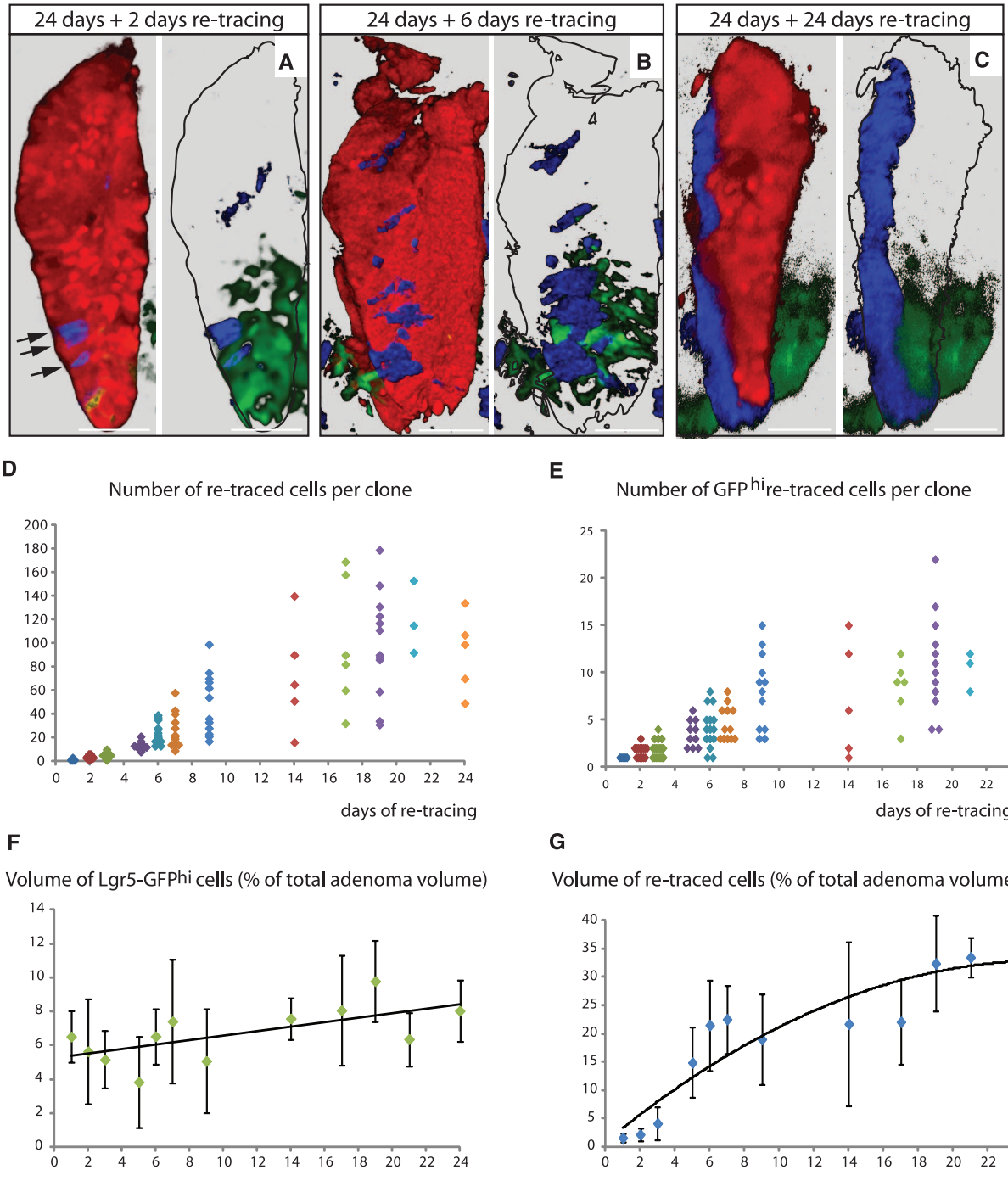

Fig. 3. Retracing of Lgr5^{+} adenoma cells. (**A**) *Apc*-deficient adenomas were allowed to develop for 24 days in *Lgr5-EGFP-Ires-CreERT2/Apc$^{fl/fl}$/R26R-Confetti* mice before retracing of Lgr5^{+} adenoma cells was induced. Two days after retracing, CFP [cyan fluorescent protein (blue)]–positive cells (arrows) were observed at the bottom of a red adenoma segment. Lgr5-EGFP is shown in green. (**B**) Six days after retracing, blue ribbons of cells were present within red adenoma segments. (**C**) Twenty-four days after retracing, blue cells comprised a large part of the adenoma. (**D** and **E**) Quantification of the total amounts of retraced cells (D) and the amounts of Lgr5-GFP^{hi+} retraced cells (E) over time. (**F**) Calculated volume of GFP^{hi} cells as a percentage of the total volume of the adenoma segment. Error bars represent SEM. A linear trend line is given, R^2 = 0.41. (**G**) Calculated volume of the retraced cells as a percentage of the total volume of the adenoma segment. Error bars represent SEM. A second-order polynomial trend line is given, R^2 = 0.86.

Downloaded from www.sciencemag.org on August 12, 2012

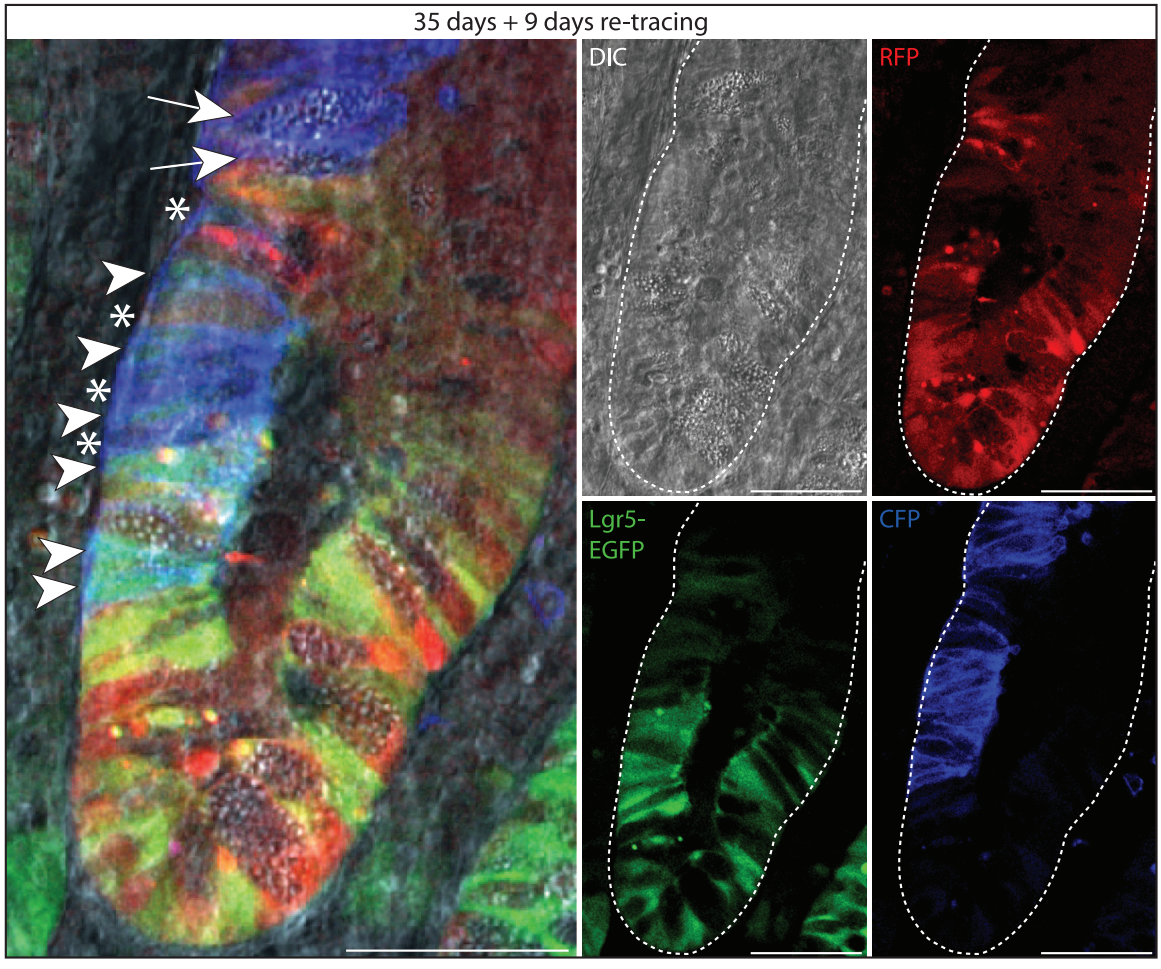

Fig. 4. Lgr5^{+} adenoma cells expand and give rise to adenoma Paneth cells. A red adenoma segment retraced for 9 days after 35 days of adenoma development in a *Lgr5-EGFP-Ires-CreERT2/Apc$^{fl/fl}$/R26R-Confetti* mouse. The left image is an overlay of four channels; DIC is shown in gray, the original segment in red, Lgr5^{+} cells in green, and the retraced cells in blue. Within the red segment, a blue clone appears, originating at the Lgr5-EGFP^{+} base of the cryptlike structure. Multiple Lgr5-GFP^{+} adenoma cells occur within the clonal ribbon (arrowhead), demonstrating the expansion of Lgr5^{+} adenoma cells. In addition, at least two blue Paneth cells (arrows) and multiple blue Lgr5^{-} cells, resembling transit-amplifying cells (asterisks), are present. Scale bars, 50 μm.

(*3*). From day 9 to day 24 after retracing, the blue cells expanded to compose up to 30% of the volume of the adenomas (Fig. 3, C and G). A quantification of clone size over time is given in Fig. 3D. The number of Lgr5-GFP^{hi} stem cells within the retraced population also increased over time, indicating that Lgr5^{+} adenoma stem cells clonally expanded within established adenomas (Fig. 3E). The total number of Lgr5-GFP^{hi} cells comprised a minority of the adenoma cells. We found that around 5 to 10% of the adenoma cells were Lgr5-GFP^{hi} (Fig. 3F). This number is similar to that of normal crypts, which consist of 150 to 200 cells and harbor about 15 stem cells each, thus reinforcing the notion that adenomas retain characteristics of the crypt stem cell niche.

To address whether Lgr5-GFP^{hi} adenoma cells are able to generate all cell types of the adenoma, we studied the phenotype of individual cells within the clonal offspring of an Lgr5^{+} adenoma cell. As an example, Fig. 4 depicts a red adenoma after 35 days of tracing, with a subsequent retracing for 9 days, in which an Lgr5^{+} adenoma cell gave rise to a blue ribbonlike clone (see also fig. S5). Multiple Lgr5-GFP^{+} adenoma cells were observed within the clonal ribbon (arrowheads), demonstrating the production of additional Lgr5^{+} adenoma cells within the ribbon. In addition, at least two blue Paneth cells (arrows) and multiple blue Lgr5^{-} cells, resembling transit-amplifying cells (asterisks), could be observed after 9 days of retracing within the clonal ribbonlike structure. These results indicate that Lgr5^{+} adenoma cells give rise to the other cell types in the adenoma. Combined with the observation that large parts of an adenoma can emerge from a single Lgr5^{+} adenoma cell, these observations qualify these cells as the multipotent stem cells of the adenoma.

The original studies that propose the existence of cancer stem cells in human colorectal cancer have their basis in transplantation of sorted cell populations into immunodeficient mice (*16*–*18*). The manipulations required for sorting, combined with the xenotransplantation setting, impose inherent limitations to the interpretation of the outcome of this assay (*19*). In an alternative approach, single-cell sorting of cultured primary colorectal cancers has been used to demonstrate that about 1 in 20 cells has the capacity in vitro of multilineage differentiation, considered an attribute of stem cells (*20*). In a follow-up study, this culture-based assay was combined with the classic xenograft approach to demonstrate that colon cancer stem cells display high Wnt pathway activity (*21*). The stem cell marker used in the current study, Lgr5, is encoded by a Wnt target gene and itself constitutes a Wnt receptor component (*22*).

Batlle and colleagues used markers enriched in normal colon Lgr5^{+} stem cells to visualize a stemlike cell population in human colon cancers, residing at the base of structures that resemble normal crypts (*21*). Indeed, the presence of Lgr5^{+} stem cells and of all differentiated lineages within colon cancers was confirmed by single-cell polymerase chain reaction (*23*). These latter two studies imply that our current functional observations on Lgr5^{+} stem cells in mouse adenomas extend to human colon carcinomas. Although adenomas represent only the first stage of intestinal tumorigenesis, the composition of these tumors, as revealed in this study, is fully compatible with the original notion of Pierce and Speers (*24*) that "carcinomas are caricatures of tissue renewal, in that they are composed of a mixture of malignant stem cells, which have a marked capacity for proliferation and a limited capacity for differentiation under normal homeostatic conditions, and of the differentiated, possibly benign, progeny of these malignant cells."

References and Notes

1. E. R. Fearon, B. Vogelstein, *Cell* **61**, 759 (1990).
2. K. W. Kinzler, B. Vogelstein, *Cell* **87**, 159 (1996).
3. N. Barker *et al.*, *Nature* **449**, 1003 (2007).
4. N. Barker *et al.*, *Nature* **457**, 608 (2009).
5. L. Zhu *et al.*, *Nature* **457**, 603 (2009).
6. H. J. Snippert *et al.*, *Cell* **143**, 134 (2010).

Downloaded from www.sciencemag.org on August 12, 2012

7. H. Ireland, C. Houghton, L. Howard, D. J. Winton, *Dev. Dyn.* **233**, 1332 (2005).
8. A. J. Merritt, K. A. Gould, W. F. Dove, *Proc. Natl. Acad. Sci. U.S.A.* **94**, 13927 (1997).
9. M. R. Novelli *et al.*, *Science* **272**, 1187 (1996).
10. T. Sato *et al.*, *Nature* **469**, 415 (2011).
11. M. E. Rothenberg *et al.*, *Gastroenterology* **142**, 1195 (2012).
12. D. A. Tuveson *et al.*, *Cancer Cell* **5**, 375 (2004).
13. J. Muñoz *et al.*, *EMBO J.* **31**, 3079 (2012).
14. T. Sato *et al.*, *Nature* **459**, 262 (2009).
15. T. Sato *et al.*, *Gastroenterology* **141**, 1762 (2011).
16. C. A. O'Brien, A. Pollett, S. Gallinger, J. E. Dick, *Nature* **445**, 106 (2007).
17. L. Ricci-Vitiani *et al.*, *Nature* **445**, 111 (2007).
18. P. Dalerba *et al.*, *Proc. Natl. Acad. Sci. U.S.A.* **104**, 10158 (2007).
19. H. Clevers, *Nat. Med.* **17**, 313 (2011).
20. L. Vermeulen *et al.*, *Proc. Natl. Acad. Sci. U.S.A.* **105**, 13427 (2008).
21. A. Merlos-Suárez *et al.*, *Cell Stem Cell* **8**, 511 (2011).
22. W. de Lau *et al.*, *Nature* **476**, 293 (2011).
23. P. Dalerba *et al.*, *Nat. Biotechnol.* **29**, 1120 (2011).
24. G. B. Pierce, W. C. Speers, *Cancer Res.* **48**, 1996 (1988).

Acknowledgments: We thank C. Kroon-Veenboer for help with mouse experiments. A.G.S and H.J.S. were funded by KWF (the Dutch Cancer Society); D.E.S. by CBG (the Centre for Biomedical Genetics); and M.vdB., J.vE., and M.vdW. by TI Pharma. Array data sets are deposited at Gene Expression Omnibus (accession no. GSE37926).

Supplementary Materials

www.sciencemag.org/cgi/content/full/science.1224676/DC1
Materials and Methods
Figs. S1 to S5
References (*25*, *26*)

18 January 2012; accepted 22 June 2012
Published online 1 August 2012;
10.1126/science.1224676

Closed-Loop Control of Epilepsy by Transcranial Electrical Stimulation

Antal Berényi,[1,2,3] Mariano Belluscio,[1] Dun Mao,[1] György Buzsáki[1,2]*

Many neurological and psychiatric diseases are associated with clinically detectable, altered brain dynamics. The aberrant brain activity, in principle, can be restored through electrical stimulation. In epilepsies, abnormal patterns emerge intermittently, and therefore, a closed-loop feedback brain control that leaves other aspects of brain functions unaffected is desirable. Here, we demonstrate that seizure-triggered, feedback transcranial electrical stimulation (TES) can dramatically reduce spike-and-wave episodes in a rodent model of generalized epilepsy. Closed-loop TES can be an effective clinical tool to reduce pathological brain patterns in drug-resistant patients.

A successful, although not well-understood, therapy in drug-resistant cases of Parkinson's disease and depression is deep brain stimulation (*1*–*3*), in which high-frequency stimulation is applied continuously. In many diseases, such as epilepsies, events recur unpredictably and often are separated by long interictal intervals (*4*–*6*). In such instances, a closed-loop, transient feedback control could abort seizure episodes without inducing detrimental side effects of continuous stimulation (*7*–*13*). We attempted to achieve seizure control by means of closed-loop transcranial electrical stimulation (TES) in a rodent model of generalized ("petit mal") epilepsy (*14*, *15*) because previous experiments have shown that even very weak TES can reliably entrain neurons in widespread cortical areas (*16*–*20*).

We first demonstrated the effect of TES on cortical excitability. Local field potentials (LFPs) and multiple-unit activity (MUA) were recorded by chronically implanted tripolar electrodes (Fig. 1A) and placed in the deep and superficial layers of the frontal and parietal cortical areas (*21*). TES was applied either between the left and right

[1]Center for Molecular and Behavioral Neuroscience, Rutgers University, Newark, NJ 07102, USA. [2]Neuroscience Institute, School of Medicine, New York University, New York, NY 10016, USA. [3]Department of Physiology, University of Szeged, Szeged, H-6720, Hungary.

*To whom correspondence should be addressed. E-mail: gyorgy.buzsaki@nyumc.org

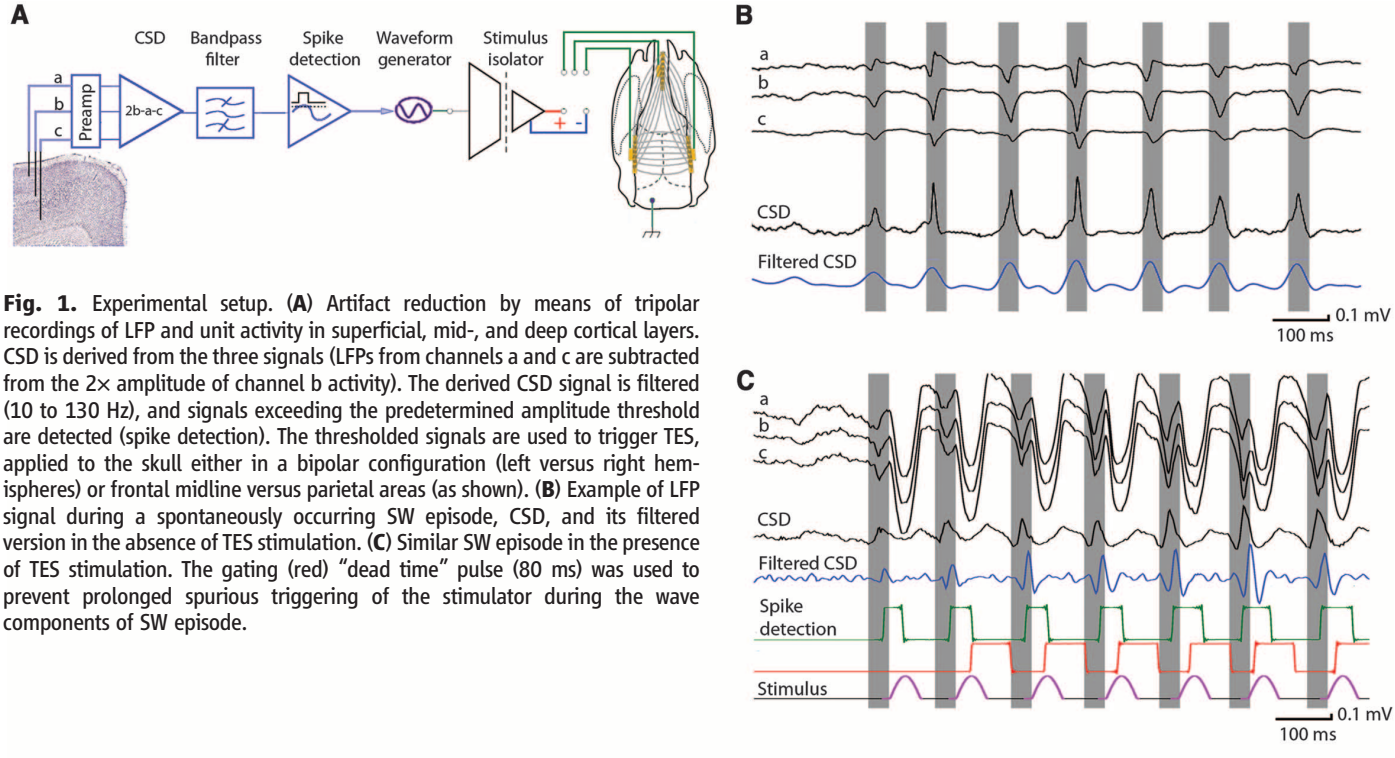

Fig. 1. Experimental setup. (**A**) Artifact reduction by means of tripolar recordings of LFP and unit activity in superficial, mid-, and deep cortical layers. CSD is derived from the three signals (LFPs from channels a and c are subtracted from the 2× amplitude of channel b activity). The derived CSD signal is filtered (10 to 130 Hz), and signals exceeding the predetermined amplitude threshold are detected (spike detection). The thresholded signals are used to trigger TES, applied to the skull either in a bipolar configuration (left versus right hemispheres) or frontal midline versus parietal areas (as shown). (**B**) Example of LFP signal during a spontaneously occurring SW episode, CSD, and its filtered version in the absence of TES stimulation. (**C**) Similar SW episode in the presence of TES stimulation. The gating (red) "dead time" pulse (80 ms) was used to prevent prolonged spurious triggering of the stimulator during the wave components of SW episode.

Downloaded from www.sciencemag.org on August 12, 2012